

Article

On the Design of Aeroelastically Scaled Models of High Aspect-Ratio Wings

Frederico Afonso ¹, Mónica Coelho ², José Vale ³, Fernando Lau ¹ and Afzal Suleman ^{1,3,*}

¹ IDMEC, Instituto Superior Técnico, Universidade de Lisboa, 1049-001 Lisboa, Portugal; frederico.afonso@tecnico.ulisboa.pt (F.A.); lau@tecnico.ulisboa.pt (F.L.)

² Instituto Superior Técnico, Universidade de Lisboa, Lisboa, 1049-001 Lisboa, Portugal; amonicalimacoelho@gmail.com

³ Department of Mechanical Engineering, University of Victoria, PO Box 1700, Stn. CSC, Victoria, BC V8W 2Y2, Canada; joselobodovale@uvic.ca

* Correspondence: suleman@uvic.ca (A.S)

Received: 6 October 2020; Accepted: 16 November 2020; Published: 18 November 2020



Abstract: Recently, innovative aircraft designs were proposed to improve aerodynamic performance. Examples include high aspect ratio wings to reduce the aerodynamic induced drag to achieve lower fuel consumption. Such solution when combined with a lightweight structure may lead to aeroelastic instabilities such as flutter at lower air speeds compared to more conventional wing designs. Therefore, in order to ensure safe flight operation, it is important to study the aeroelastic behavior of the wing throughout the flight envelope. This can be achieved by either experimental or computational work. Experimental wind tunnel and scaled flight test models need to exhibit similar aeroelastic behavior to the full scale air vehicle. In this paper, three different aeroelastic scaling strategies are formulated and applied to a flexible high aspect-ratio wing. These scaling strategies are first evaluated in terms of their ability to generate reduced models with the intended representations of the aerodynamic, structural and inertial characteristics. Next, they are assessed in terms of their potential in representing the unsteady non-linear aeroelastic behavior in three different flight conditions. The scaled models engineered by exactly scaling down the internal structure suitably represent the intended aeroelastic behavior and allow the performance assessment for the entire flight envelope. However, since both the flight and wind tunnel models are constrained by physical and budgetary limitations, custom built structural models are more likely to be selected. However, the latter ones are less promising to study the entire flight envelope.

Keywords: aeroelastic scaling; nonlinear aeroelasticity; high aspect-ratio wings; fluid-structure interaction

1. Introduction

One of the design solutions for improving the aerodynamic performance of commercial jetliners is to increase the aspect-ratio of the wing such that a reduction in the induced drag is obtained. Aspect-ratio increase is usually achieved by a compromise in chord reduction and span increase that enables aerodynamic advantages at typical operating conditions, namely in cruise and high g's maneuvers, without a severe increase of the structural weight. This design solution has however an impact on the wing's structure which is now more prone to higher deflections and root bending moments with the increase of wing span, which may result in geometric nonlinearities [1–9]. Hazardous aeroelastic phenomena such as flutter may arise from this higher flexibility in the flight envelope. Hence, the importance of studying aircraft aeroelastic behavior computationally and devising sub-scale models that are representative of the aeroelastic behavior of full size wing designs to enable the study of these new designs [10–12].

The topic of aeroelastic scaling is not new and significant efforts were made over recent decades. In fact, there are recent survey papers that cover the efforts carried out in aeroelastic scaling, but in general their focus are in broader subjects such as structural engineering [13,14] or aerodynamics [15]. Coutinho et al. [13] have presented an overview of the efforts done to build reduced scale models for structural engineering applications up to 2015. The recent paper from Casaburo et al. [14] which covers the main similitude methods for structural engineering, where simple and complex structures from different engineering fields are discussed, expands the previous revision paper. In a more recent paper [15], the author surveys wind tunnel models designed by recurring to additive manufacturing technologies, including some aeroelastic models built to study steady and unsteady aeroelastic phenomena.

There are some papers wherein the goal is set at devising aeroelastically scaled models of high aspect-ratio wings to study their behavior in flight [16–19] or in wind tunnel [20–22]. In the vast majority of the research articles in aeroelastic scaling, optimization is used as a numerical tool to build sub-scale models with the same structural dynamic behavior as their full size counterpart [17,20,21,23–27]. To achieve this, some authors set as design variables the dimensions of a predefined sub-scale internal structure and in some case mass points with the goal of reaching the same stiffness and mass characteristics of the full scale model, which requires solving at each optimization iteration a modal analysis. The mass points are sometimes defined in a second optimization loop, which succeeds a first optimization problem set to match the stiffness properties, evaluated using a static analysis, such as in [17,24,27]. Different objective functions and constraints are defined to replicate the dynamic properties in the sub-scale models, such as static deflection to a prescribed load, natural frequencies and corresponding mode shape, reduced frequencies, overall mass, and flutter speed, among others. Recently, a methodology to evaluate and design dynamically scaled models was proposed based on approximate similitude [28].

Nevertheless, only a few of these papers aim at studying nonlinear aeroelastic phenomena [18,19,21,25–27]. In this current work, the authors present different aeroelastic scaling strategies, for devising flight or wind tunnel models, formulated using three different sets of primary quantities to evaluate their performance in replicating the same nonlinear aeroelastic behavior of a full scale high aspect-ratio wing for different conditions in the flight envelope. This performance assessment is done and discussed in light of geometric, aerodynamic, structural, inertial, and aeroelastic (nonlinear unsteady response for three flight conditions) characteristics.

2. Methodology

The methodology section is organized as follows: (a) first the scaling strategies required to ensure aeroelastic similarity between full and scaled models are presented and discussed; (b) then the aeroelastic scaling methodology employed in this work is summarized; (c) and finally the aeroelastic framework is briefly introduced.

2.1. Aeroelastic Scaling

To aeroelastically scale a given model and before establishing scaling factors, one has to choose a set of three primary quantities encompassing mass, length and time. This choice has an impact on how well the scaled model represents its full size counterpart and is normally conditioned by several factors, especially by the purpose of the scaled model itself (i.e., for wind tunnel or flight testing) and the available budget which will dictate among others the size, mass and airspeed of the model. A suitable aeroelastic scaling is attained when the reduced model, also known as sub-scale model, mimics the structural dynamic and unsteady aerodynamic behavior of the real size model as well as the coupling behavior of these disciplines, i.e., the aeroelastic behavior. The aeroelastic behavior can be written in terms of the vector of elastic degrees of freedom $\{x\}$ as follows,

$$[M] \{\ddot{x}\} + [C] \{\dot{x}\} + [K] \{x\} = [A_M] \{\ddot{x}\} + [A_C] \{\dot{x}\} + [A_K] \{x\}, \quad (1)$$

where the left hand side terms are related to the structural dynamic behavior considering the mass [M], damping [C] and stiffness [K]; while in the right hand side the equivalent aerodynamic terms are represented, i.e., mass [A_M], damping [A_C] and [A_K] stiffness.

Herein, three different sets of primary quantities are investigated to evaluate their applicability in devising aeroelastically scaled models for high aspect-ratio wings:

1. Density (ρ), Velocity (v) and Span (b);
2. Frequency (ω), Mass (m) and Span (b);
3. Pressure (p), Density (ρ) and Span (b).

The first set is a common choice for devising flight test models since normally size, engine power and air properties choices are very limited, although it can also be used for designing aeroelastically scaled wind tunnel models. Values for the primary quantities of Set 2 have to be carefully selected such that it does not result in infeasible air properties. Set 3 can be seen as a promising option if the size of the model allows for manufacturing an exact scale down of the internal structure since the same material can be selected (given that these primary quantities have units of pressure and density).

After establishing a set of primary quantities, the Buckingham’s II theorem [29] can then be applied to derive other relevant physical parameters by means of scaling factors (k). Length, time (t), frequency, mass, density, velocity, pressure, force (F), moment (M); and inertia (I) parameters are summarized in Table 1. The scaling factors are the result of the application of this theorem and are essential to derive the target parameters that the sub-scale model should match. The scaling factors directly associated with the primary quantities of each set, also known as independent scaling factors, are shaded and the subscripts s and r denote scaled and real size models, respectively.

Table 1. Summary of the scaling factors for the 3 sets of primary quantities. The shaded cells correspond to the selected primary quantities in each set.

Parameter	Set 1	Set 2	Set 3
Length, k_l	$\frac{b_s}{b_r}$	$\frac{b_s}{b_r}$	$\frac{b_s}{b_r}$
Time, k_t	$\frac{k_l}{k_v}$	$\frac{1}{k_\omega}$	$\sqrt{\frac{k_\rho k_l^2}{k_p}}$
Frequency, k_ω	$\frac{k_v}{k_l}$	$\frac{\omega_s}{\omega_r}$	$\sqrt{\frac{k_p}{k_\rho k_l^2}}$
Mass, k_m	$k_\rho k_l^3$	$\frac{m_s}{m_r}$	$k_\rho k_l^3$
Density, k_ρ	$\frac{\rho_s}{\rho_r}$	$\frac{k_m}{k_l^3}$	$\frac{\rho_s}{\rho_r}$
Velocity, k_v	$\frac{v_s}{v_r}$	$k_\omega k_l$	$\sqrt{\frac{k_p}{k_\rho}}$
Pressure, k_p	$k_\rho k_v^2$	$k_m k_l^3 k_\omega^2$	$\frac{p_s}{p_r}$
Force, k_F	$k_\rho k_v^2 k_l^2$	$k_m k_l k_\omega^2$	$k_p k_l^2$
Moment, k_M	$k_\rho k_v^2 k_l^3$	$k_m k_l^2 k_\omega^2$	$k_p k_l^3$
Inertia, k_I	$k_\rho k_l^5$	$k_m k_l^2$	$k_\rho k_l^5$

These scaling factors should ensure both aerodynamic and dynamic similarities besides the obvious geometric similarity. The latter is achieved in all three sets.

Starting with aerodynamic similarity, despite the external geometry being the same it is difficult to completely achieve this similarity since both Reynolds (Re) and Mach (Ma) numbers are not necessarily maintained. The task of matching these two dimensionless numbers in an aeroelastically scaled model is deemed very difficult and it is normally not done; it usually requires a compromise between model size (mass and length) and air properties (namely its density and temperature) which is usually not possible, especially if flight testing is sought. This shortcoming has influence on the viscous (Reynolds) and compressibility effects (Mach) of the scaled model. Sometimes roughness is added to the scaled model to induce separation at the same location of the full size computational model [30]. Nevertheless, accordingly to Pittit et al. [31] the Reynolds number is generally of minor importance

for evaluating aeroelastic effects on main wings, as will be the case in study here; and accordingly to Ricciardi et al. [25] the Mach number is also assumed to present a small influence. Mach number similarity is enabled with Set 3, which might be useful if one desires to evaluate possible shock wave variation on the wing induced by the aeroelastic behavior, although this would be very difficult to achieve in a sub-scale flight test model. Therefore, in this work the similarity of both Reynolds and Mach numbers is set as a desirable goal, but not essential.

In what concerns the dynamic behavior, its similarity, also known as dynamic scaling, is reached when the target modal parameters, i.e., natural frequencies and associated mode shapes and damping ratios, are matched. In the case of exactly scaling the internal structure and using the same material, this similarity is automatically attained; however, since it is not often the case, for instance due to manufacturability issues, an optimization problem is normally employed to design a structure that can match the first target natural frequencies and associated mode shapes with those of the real model. Damping ratios are more difficult to account for in computational models and due to this reason they are rarely used and will not be considered in this work.

There are several strategies to dynamically scale a model resorting to optimization and starting with a simplified internal structure, as recommended by Bisplinghoff et al. [32], such as those presented in [17,18,25,27], but in this work only the method depicted in Figure 1 from [27] is used, but with different objective function and constraints established.

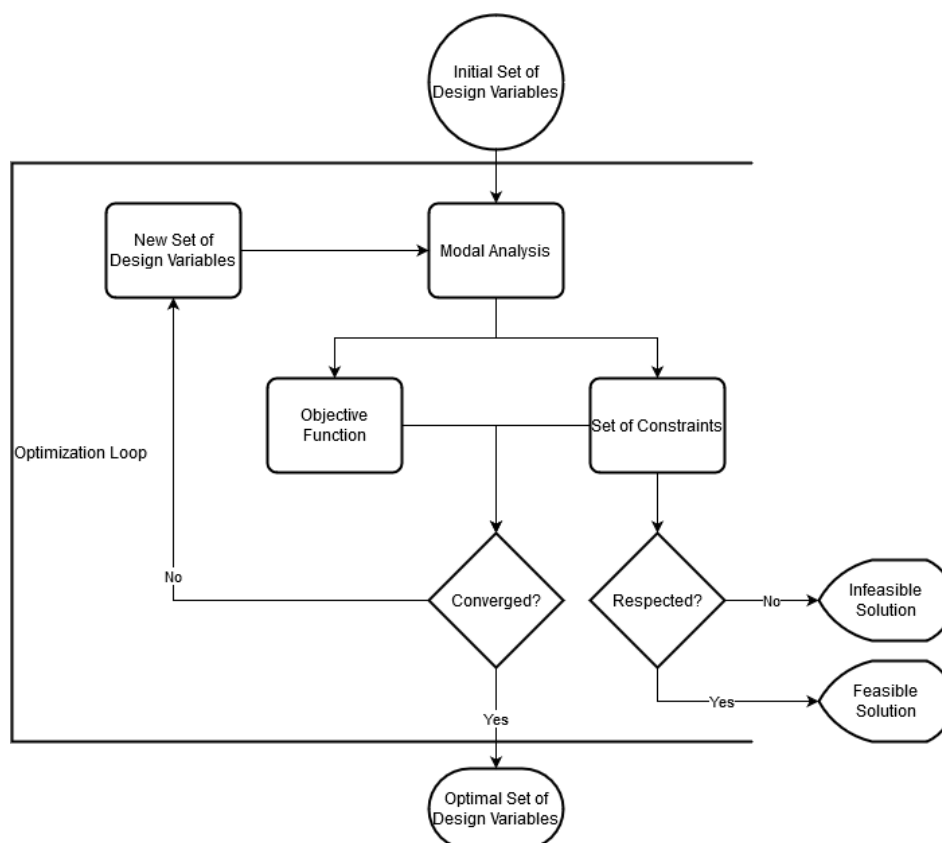


Figure 1. Scaling methodology.

A generic problem statement for the scaling methodology selected can be formulated as follows,

$$\begin{aligned}
 & \text{minimize} && \sqrt{\frac{1}{N} \sum_{i=1}^N (f_i(x) - f_i^t)^2} + \sqrt{\frac{1}{N} \frac{1}{N} \sum_{i=1}^N \sum_{j=1}^N (\text{MAC}_{i,j}(x) - \text{MAC}_{i,j}^t)^2} \\
 & \text{with respect to} && x \\
 & \text{subject to} && (f_i(x) - f_i^t) / f_i^t - 0.05 \leq 0 \quad \text{with } i = 1 : N \\
 & && (m(x) - m^t) / m^t - 0.05 \leq 0 \\
 & && (I_{i,j}(x) - I_{i,j}^t) / I_{i,j}^t - 0.05 \leq 0 \quad \text{with } i = 1 : 3 \text{ and } j = 1 : 3
 \end{aligned} \tag{2}$$

where f_i is the i th natural frequency of the structure; N is the number of mode shapes to match; superscript t denotes target value for the given parameter; m and I represent the overall mass and the inertia tensor of the structure, respectively; x is a set of design variables; and MAC is the Modal Assurance Criterium matrix, which is a metric to evaluate how two different sets of mode shapes, in this case the target and the obtained ones, are correlated:

$$\text{MAC} = \frac{\phi^T \times \phi_t}{(\phi^T \times \phi) (\phi_t^T \times \phi_t)}, \tag{3}$$

where ϕ is a matrix with a set of mode shapes. To avoid nomenclature misunderstanding, t referring to target is now a subscript since T denotes transpose. Two different sets of mode shapes are said to be perfectly correlated when the MAC matrix is an identity matrix.

The optimization problem (Equation (2)) is posed differently to that from [27] where direct mode matching was preferred instead of MAC in the objective function definition and the inertia tensor of the structure was added to the set of constraints. The former was chosen to improve numerical performance, while the latter accounts for the inertial properties, which is expected to be more relevant when flexibility effects are higher in the scaled model, which is the case of high aspect-ratio wings.

Other dimensionless parameters that should be kept in the scaled model are the reduced frequencies (κ) and the Froude number (Fr). Reduced frequencies are computed for a given airspeed considering the natural frequencies and the wing span:

$$\kappa = \frac{fb}{v}. \tag{4}$$

Froude number accordingly to Wan and Cesnik [19] should be matched to ensure similarity when flexibility effects are relevant to be analyzed in the devised model; this parameter is given as follows:

$$Fr = \frac{v}{\sqrt{bg}}, \tag{5}$$

where g is the acceleration of gravity.

2.2. Methodology

The following methodology was the one applied in this work:

1. Build a full size wing model in the aeroelastic framework and run time domain simulations for three flight conditions (cruise, hold and alternate);
2. Derive the scaling factors and the resulting target parameters to be matched by the sub-scale models, considering 3 different sets of primary quantities;
3. Apply a scaling methodology resorting to optimization with the aim at reaching the same dynamic scaling of the full size wing model;

4. Run nonlinear unsteady simulations to predict the nonlinear aeroelastic response of the 3 scaled models and compare with the responses estimated for the initial wing model, i.e., the target responses for cruise, hold and alternate flight conditions.

2.3. Aeroelastic Framework

An in-house nonlinear aeroelastic framework described in [33,34] was used in this work. This framework is capable of analyzing flexibility effects on high aspect-ratio wings in the time domain considering both constrained, i.e., simulating wind tunnel conditions, and unconstrained i.e., emulating free-flight conditions, models. For this task, the code was enabled with a Fluid-Structure Interaction (FSI) algorithm responsible for coupling the structural and aerodynamic models by recurring to a loosely coupled scheme (where despite fluid and structure models being solved separately, the solution only advances in time when convergence between fluid and structure models is reached) that ensures consistency, but not energy conservation. Despite the use of low-medium fidelity aerodynamic (3D panel method with viscous and compressibility corrections) and structural (3D condensed beam model based on wing-box mass and inertia calculations) models, their applicability to preliminary design is adequate since they capture the main physical phenomena and allow exploring the design space [35,36]. The aerodynamic, structural and aeroelastic models were benchmarked [33,34] with existing data available in the literature. Furthermore, the application of this framework to estimate the aeroelastic behavior of both full and reduced size models ensures comparability between these models. Another feature available is the optimization capability [37], which for this work is necessary to design the structure of the sub-scale models such that it ensures dynamic similarity (i.e., to solve Equation (2)).

3. Wing Model

3.1. Full Size Model

For the wing model, such as in [27], a modified version of the main wing of the NOVEMOR project [38] was employed, but with an even higher aspect-ratio. The unmodified wing with an aspect-ratio and area of 9 and 110 m², respectively, was stretched to increase the aspect-ratio to 16. For this task, the wing area and the angles of leading edge sweep and dihedral were kept unchanged, while the planform was altered by increasing the span and reducing the chord in a proportional way, i.e., indexed to the original span and mean aerodynamic chord. This geometrical modification combined with the chosen internal layout allows the wing to already present flexibility effects during normal operating conditions (e.g., at cruise). A simplified aluminum made wing box (with density of 2700 kg/m³, Young's modulus of 70 GPa and Poisson's ratio of 0.33) comprised between 25 and 75% of the local chord along the entire span was defined as the internal structure and the thicknesses of the spars and skins were assumed uniformed with values of 28 mm and 5.6 mm, respectively. This is an assumption made for this work. A different thickness distribution along the wingspan could have been made for the spar and skin, as well as a different material. However, the applicability of the scaling strategies here applied would not change. Only the inertial properties of the wing model would change and as a consequence the structural and aeroelastic behavior would also change, thus resulting in different target values for the scaled models to match. The main geometric characteristics of the modified wing are presented in Table 2 and its planform depicted in Figure 2.

Before proceeding with the scaling of this full size wing model, nonlinear aeroelastic time domain responses are estimated considering the already mentioned three different flight conditions: cruise; hold; and alternate (see Table 3). To obtain the unsteady aeroelastic responses for each of these flight conditions, the aeroelastic framework above mentioned was employed. The computational models for the aerodynamics and structures were defined based on a convergence study and have the following characteristics: an aerodynamic mesh built with an uniform distribution in the span direction (28 divisions), a cosine distribution in the chord direction (divisions) and an uniform wake of 100 chords length; structural mesh composed of 50 equally spaced nonlinear 3D beam finite elements.

In the aeroelastic model the wing was set to be constrained at its root and the simulations start from an undeformed state; then the wing model is released into a constant airflow corresponding to the chosen flight condition, thus emulating a wind tunnel model with a sudden wind on condition. Despite this choice to estimate the aeroelastic response of both full and reduced models, the initial conditions could have been changed to simulate a flight test condition.

Table 2. Main geometric characteristics of the modified wing.

Characteristic	Value
Area (m ²)	110
Aspect-ratio (-)	16
Span (m)	41.95
Mean Aerodynamic Chord (m)	2.62
Root Chord (m)	4.95
Inboard Wing Half Semi-span (m)	8.24
Break Chord (m)	2.61
Outboard Wing Half Semi-span (m)	12.73
Tip Chord (m)	1.13
Dihedral Angle (deg)	4.4
Leading Edge Sweep Angle (deg)	27.5

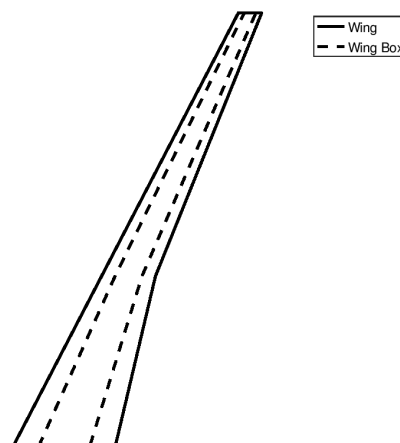


Figure 2. Wing model.

Table 3. Flight conditions.

	Cruise	Hold	Alternate
Mach (-)	0.78	0.5	0.3
Altitude (m)	11582	5486	610
Air density (kg/m ³)	0.332	0.698	1.155
Velocity (m/s)	230	159	101
Trim lift coefficient (-)	0.588	0.584	0.872
Trim angle of attack (deg)	5.36	5.33	7.95

3.2. Reduced Scale Models

The definition of each primary quantity value for each Set to design aeroelastically scaled models was mainly based on having a wing semi-span large enough to accommodate the internal structure and the necessary instrumentation for flight testing, but not larger than 2.5 m to disable its testing on some closed-loop wind tunnel facilities; utilizing a material that potentiates the usage of 3D printing

technology for building cheaper but yet complex geometries [39,40] when a direct scale down of the geometry is not possible; and enabling flight or wind tunnel testing.

Based on the above rationale, a length scale of 1/10th resulting in a wing semi-span lower than 2.2 m was selected for all the analyzed sets of primary quantities; aluminum and nylon (Young's modulus of 1.27 GPa, shear modulus of 0.3 GPa and density of 1010 kg/m³) materials were selected for Sets 3 and Sets 1 and 2, respectively. For Sets 2 and 3 the air density and speed were obtained by the application of the scaling factor, although for Set 1 they were set to 1.225 kg/m³ and 50 m/s, respectively, since it is possible to choose them in this Set. Considering the choices of values for the primary quantities and the scaling factors derived from them (given in Table 4), the main geometric, aerodynamic and structural parameters for each reduced model can be determined. Both geometric and aerodynamic parameters are inputs for the design of the reduced size models, while the structural parameters will be set as targets to be obtained; these are summarized in Table 5, from which one can add some comments regarding similarities between sub-scale models and full size model:

- Geometric similarity is achieved with all the Sets of primary quantities at an external level, while only Set 3 provides internal geometric similarity due to the possibility of manufacturing the wing box structure using the same material (with thickness of 2.8 mm and 0.56 mm);
- Reynolds number is not matched using any of the Sets of primary quantities (Set 3 is the one that is closest to the full size model) which means that the viscous effects will not be sufficiently represented in the sub-scale models, especially for the Set 2 for which a low Reynolds number was derived; as mentioned before Reynolds number is not considered to be of major importance for aeroelastic problems on the wing [31], although if deemed important for a given flight condition skin roughness can be changed to induce transition to turbulent flow as suggested in [30];
- Compressibility effects will only be accurately represented when using Set 3; it is worth noting that the interaction between viscous and compressibility effects, if exists, will not be adequately captured since Reynolds number is not matched;
- Dynamic similarity is immediately achieved by using Set 3 of primary quantities, because besides geometric similarity being possible both pressure and density are selected as primary quantities which enables the usage of the same material as in the full size model;
- Froude number similarity is another similarity parameter that is not achieved with any of the Sets of primary quantities, although Set 2 provides the closest value.

Table 4. Summary of the resulting scaling factors for the 3 sets of primary quantities. The shaded cells correspond to the primary quantities chosen for each set.

Parameter	Set 1	Set 2	Set 3
Length, k_l	0.1	0.1	0.1
Time, k_t	0.4603	0.4541	0.1
Frequency, k_ω	2.1725	2.2023	10
Mass, k_m	0.0037	3.7407×10^{-4}	0.001
Density, k_ρ	1	0.3741	1
Velocity, k_v	0.2172	0.2202	0.3162
Pressure, k_p	0.1741	0.0181	1
Force, k_F	0.0017	1.8143×10^{-4}	0.01
Moment, k_M	0.0002	1.8143×10^{-5}	0.001
Inertia, k_I	3.6899×10^{-5}	3.7407×10^{-6}	1.0×10^{-5}

Table 5. Summary of the geometric, aerodynamic and structural parameters for the 3 sets of primary quantities.

Parameter	Full-Size	Set 1	Set 2	Set 3
Wing semi-span (m)	20.975	2.0975	2.0975	2.975
Mean aerodynamic chord (m)	2.62	0.262	0.262	0.262
Wing area (m ²)	110	1.1	1.1	1.1
Air density (kg/m ³)	0.332	1.225	0.124	0.332
Air speed (m/s)	230	50	51	230
Mach number (-)	0.78	0.15	0.17	0.78
Reynolds number (-)	13,987,903	1,121,297	115,235	1,398,790
Trim lift coefficient (-)	0.588	0.588	0.588	0.588
Trim angle of attack (deg)	5.36	5.36	5.36	5.36
Mass (kg)	1874	6.915	0.701	1.874
I _{xx} (kg.m ²)	183,312	6.764	0.686	1.833
I _{yy} (kg.m ²)	59,838	2.208	0.224	0.598
I _{zz} (kg.m ²)	240,147	8.861	0.898	2.401
I _{xy} (kg.m ²)	-100,368	-3.704	-0.375	-1.004
I _{xz} (kg.m ²)	8915	0.329	0.033	0.089
I _{yz} (kg.m ²)	-16,459	-0.607	-0.062	-0.165
Froude number (-)	11.4	20.3	7.9	35.9

Overall mass and inertia moments are set as targets to be matched in the structural design of the scaled models to reinforce the need to account for flexibility effects, due to the slenderness characteristic of high aspect-ratio wings.

4. Results

4.1. Aeroelastic Scaling

The previous section sets the targets to be met in the structural design of the sub-scale models. These targets, i.e., natural frequencies, correlation between mode shapes, overall mass and inertia moments compose the objective function and set of constraints of the optimization problem to be solved (Equation (2)) for each set of primary quantities. The selected design variables are related to the wing box characteristics: thickness of the leading and trailing edge spars at root, break and tip sections (linear interpolation is considered between sections); thickness of the wing skin, assumed uniformed, at root, break and tip sections (again linear interpolation is considered between sections); initial and final local chord positions of the wing box at each section (root, break and tip). A total of 15 design variables (x in Equation (2)) are thus used to design the internal structure of the sub-scale models.

Starting with Set 1, for which span, density and velocity were established as primary quantities, both aerodynamics and structural results are far from the defined target values, as one can notice from Table 6. It is worth recalling that the target values are obtained by applying the scaling factors of Table 4 to the corresponding parameter and set. Regarding aerodynamics, the lower velocity ($v = 50$ m/s set for cruise) and the smaller scale (10 times smaller when compared with the full size model) have dictated the reduction of the Mach and Reynolds numbers with consequences on the aerodynamic coefficients (lift, drag and pitch moment), specially for the faster flight conditions, where compressibility effects have more influence as expected. Another aerodynamic problem with this Set of primary quantities is related to the exploration of the flight envelope: if we define, as we did for cruise, the speed and air density at 50 m/s and sea level conditions, respectively, for the remaining conditions (alternate and hold) the air densities will be higher which will be very difficult to achieve in a flight testing campaign, despite the lower speeds. Thus, this Set might only be appropriate for evaluating aeroelastic behavior for a given flight condition. In what concerns the structure, the different characteristics of the materials between full and scaled models combined with a relatively simple

structural layout and a low number of design variables have not allowed achieving the same structural dynamic behavior, despite the relative differences between full and scaled models inertial properties being lower than 12.4%. If one computes the reduced frequencies, they will also be far from the ones calculated for the full size model. From the authors experience [27] with this Set it should be possible to improve the structural dynamic behavior with a higher number of design variables and recurring to mass points to tune the sub-scale model.

Table 6. Aerodynamics, structural and inertial results obtained using Set 1.

Parameter	Full Size	Target	Scaled	Difference (%)
C_L @ cruise (-)	0.779	0.779	0.614	21.2
C_D @ cruise (-)	0.067	0.067	0.011	83.7
C_M @ cruise (-)	1.305	1.305	0.954	26.9
C_L @ alternate (-)	0.697	0.697	0.607	12.9
C_D @ alternate (-)	0.014	0.014	0.011	24.2
C_M @ alternate (-)	1.082	1.082	0.943	12.9
C_L @ hold (-)	0.871	0.871	0.833	4.4
C_D @ hold (-)	0.021	0.021	0.018	11.3
C_M @ hold (-)	1.381	1.381	1.321	4.4
1st Flap (Hz)	1.263	2.745	3.845	40.2
2nd Flap (Hz)	5.155	11.198	11.321	1.1
1st Chord (Hz)	5.228	11.357	11.635	2.5
3rd Flap (Hz)	11.677	25.368	23.100	8.9
2nd Chord (Hz)	20.904	45.414	24.030	47.1
4th Flap (Hz)	21.211	46.080	36.705	20.4
1st Torsion (Hz)	27.660	60.090	41.495	30.9
5th Flap (Hz)	34.253	74.412	45.931	38.3
3rd Chord (Hz)	47.553	103.308	65.918	36.2
6th Flap (Hz)	50.178	109.009	70.851	35.0
Mass (kg)	1874	6.915	7.281	5.3
I_{xx} (kg.m ²)	183,312	6.764	6.015	11.1
I_{yy} (kg.m ²)	59,838	2.208	2.008	9.1
I_{zz} (kg.m ²)	240,147	8.861	7.926	10.6
I_{xy} (kg.m ²)	-100,368	-3.704	-3.300	10.9
I_{xz} (kg.m ²)	8915	0.329	0.288	12.4
I_{yz} (kg.m ²)	-16,459	-0.607	-0.536	11.8

The selection of frequency and mass primary quantities in Set 2 has allowed for scaling the material properties from aluminum to nylon, by means of manipulating material density and Young's modulus relations through density and pressure scaling factors to establish mass and frequency scaling factors. This resulted in a close structural and inertial properties match to the target values, as one can observe from Table 7. An exception was the first torsion mode which depends on both the Young's modulus and the Poisson's ratio; this last property is not maintained hence the discrepancy that can be of relevant importance in the typical case of flutter occurring due to the coupling of bending and torsion modes. The reduced frequencies are closer (about 30% of relative difference) to those from the full size model, except again for the torsional reduced frequency which has a higher discrepancy (45% of relative difference). In what concerns aerodynamics, the same comment made for the application of Set 1 can be done to Set 2 with the aggravation of an even higher relative error for the Reynolds number, with consequences in its ineptitude to account for the existing viscous effects. As a consequence of setting density scaling factor considering only material properties, the resulting air densities for each flight condition are even lower than the ones from the full scale, for instance a density equivalent to 17,820 m of altitude is calculated. This means that for flight testing one has to fly at the equivalent altitude or using lighter gases than air in a wind tunnel facility. Both options seem expensive.

Table 7. Aerodynamics, structural and inertial results obtained using Set 2.

Parameter	Full size	Target	Scaled	Difference (%)
C_L @ cruise (-)	0.779	0.779	0.628	19.5
C_D @ cruise (-)	0.067	0.067	0.014	79.1
C_M @ cruise (-)	1.305	1.305	0.974	25.4
C_L @ alternate (-)	0.697	0.697	0.614	11.9
C_D @ alternate (-)	0.014	0.014	0.013	9.5
C_M @ alternate (-)	1.082	1.082	0.953	12.0
C_L @ hold (-)	0.871	0.871	0.836	4.0
C_D @ hold (-)	0.021	0.021	0.019	5.7
C_M @ hold (-)	1.381	1.381	1.326	4.0
1st Flap (Hz)	1.263	2.784	2.781	0.1
2nd Flap (Hz)	5.155	11.295	11.350	0.5
1st Chord (Hz)	5.228	11.490	11.503	0.1
3rd Flap (Hz)	11.677	25.621	25.710	0.4
2nd Chord (Hz)	20.904	45.788	45.988	0.4
4th Flap (Hz)	21.211	46.630	46.648	0.0
1st Torsion (Hz)	27.660	60.921	47.821	21.5
5th Flap (Hz)	34.253	75.151	75.429	0.4
3rd Chord (Hz)	47.553	104.341	105.147	0.8
6th Flap (Hz)	50.178	110.321	110.619	0.3
Mass (kg)	1874	0.701	0.702	0.2
I_{xx} (kg.m ²)	183,312	0.686	0.687	0.1
I_{yy} (kg.m ²)	59,838	0.224	0.224	0.1
I_{zz} (kg.m ²)	240,147	0.898	0.899	0.1
I_{xy} (kg.m ²)	-100,368	-0.375	-0.376	0.1
I_{xz} (kg.m ²)	8915	0.033	0.033	0.1
I_{yz} (kg.m ²)	-16,459	-0.062	-0.062	0.2

With Set 3, for which no optimization problem was needed, the inertial and structural properties, including the reduced frequencies, of the scaled model are the same as the target ones (see Table 8). When looking at the aerodynamic results, one can notice that the Mach number similarity has allowed for errors lower than 1% for lift and pitch moments coefficients. The exception was the drag coefficient which has a higher difference from the target one, although it not as important in aeroelastic problems as the lift coefficient due to its lower value when compared with the latter. This discrepancy is explained by the Reynolds number that was not maintained, but is in fact 10 times lower due to the length scaling factor used to derive the scaled model. A note to the velocities and air densities which are the same as the ones from the full scale model, i.e., the same flight condition, thus requiring the model either to fly at high altitudes or to be tested in a transonic wind tunnel with a gas mixture lighter than air. Any of these options again might be expensive. Nevertheless, this Set seems the most adequate option for devising an aeroelastically scaled model if it is possible to manufacture an exactly scale down version of the internal structure recurring to the same material and to fly at the flight condition.

Table 8. Aerodynamics, structural and inertial results obtained using Set 3.

Parameter	Full Size	Target	Scaled	Difference (%)
C_L @ cruise (-)	0.779	0.779	0.779	0.0
C_D @ cruise (-)	0.067	0.067	0.066	2.1
C_M @ cruise (-)	1.305	1.305	1.305	0.4
C_L @ alternate (-)	0.697	0.697	0.699	0.2
C_D @ alternate (-)	0.014	0.014	0.013	6.1
C_M @ alternate (-)	1.082	1.082	1.085	0.2
C_L @ hold (-)	0.871	0.871	0.872	0.1
C_D @ hold (-)	0.021	0.021	0.020	5.3
C_M @ hold (-)	1.381	1.381	1.382	0.1
1st Flap (Hz)	1.263	12.642	12.642	0.0
2nd Flap (Hz)	5.155	51.285	51.285	0.0
1st Chord (Hz)	5.228	52.174	52.174	0.0
3rd Flap (Hz)	11.677	116.340	116.340	0.0

Table 8. Cont.

Parameter	Full Size	Target	Scaled	Difference (%)
2nd Chord (Hz)	20.904	207.912	207.912	0.0
4th Flap (Hz)	21.211	211.734	211.734	0.0
1st Torsion (Hz)	27.660	276.627	276.662	0.0
5th Flap (Hz)	34.253	341.240	341.240	0.0
3rd Chord (Hz)	47.553	473.783	473.786	0.0
6th Flap (Hz)	50.178	500.939	500.942	0.0
Mass (kg)	1874	1.874	1.874	0.0
I_{xx} (kg.m ²)	183,312	1.833	1.833	0.0
I_{yy} (kg.m ²)	59,838	0.598	0.598	0.0
I_{zz} (kg.m ²)	240,147	2.401	2.401	0.0
I_{xy} (kg.m ²)	−100,368	−1.004	−1.004	0.0
I_{xz} (kg.m ²)	8915	0.089	0.089	0.0
I_{yz} (kg.m ²)	−16,459	−0.165	−0.165	0.0

4.2. Aeroelastic Response

The nonlinear aeroelastic behavior of the reduced scaled models designed with the 3 different sets of primary quantities is now estimated in the time domain and compared with the one estimated for the full size model. As mentioned before, the wing model is constrained at its root and released into a constant flow corresponding to the desired flight condition. The response at the wing tip is measured in plunge (vertical motion of the wing), pitch (wing torsion) and chord (horizontal motion) degrees of freedom. To enable the comparison between full and reduced scale models, the plunge and chord degrees of freedom are divided by the wing's semi-span and mean aerodynamic chord, respectively. A time step study was carried out using the full size wing for which a value of 0.01 s was selected in the end. The time step for the scaled models was estimated by applying the time scaling factor (corresponding to each Set) to the one used for the full scale model.

The poor matching of the aerodynamic and structural characteristics using Set 1 is clearly visible in the nonlinear aeroelastic response measured at the 3 degrees of freedom, for the 3 flight conditions, as shown in Figure 3. Similar trends are observed when the wing model is released into the constant airflow, although the behavior tends to get further apart from the full size model, especially for alternate and hold conditions.

A better correlation between full and scaled models can be observed for Set 2 in Figure 4 from the nonlinear aeroelastic responses, which seem to follow the same trends independently of the degree of freedom or the flight condition. However, the aeroelastic response of the scaled model is shifted (under estimated) when compared with the full model due to the discrepancies in the aerodynamic coefficients (which are lower for the scaled model).

As expected from the very good matching of aerodynamic, structural and inertial properties between full and scaled models using Set 3 (Table 7), the nonlinear aeroelastic responses given in Figure 5 for both models are very close with only small deviations. Since both the Mach number and the structural behavior are replicated in the scaled model for this particular case, the authors are led to believe that the source of slight deviation found in the aeroelastic behavior may be due to Reynolds number, given that it is 10 times lower in the scaled model. This issue can be mitigated as mentioned above if transition to turbulent flow is induced by means of skin roughness. The good agreement between aeroelastic responses independently of the flight conditions is a promising indication that this Set of primary quantities can be applied to devise aeroelastically scaled models, which can be tested throughout the flight envelope.

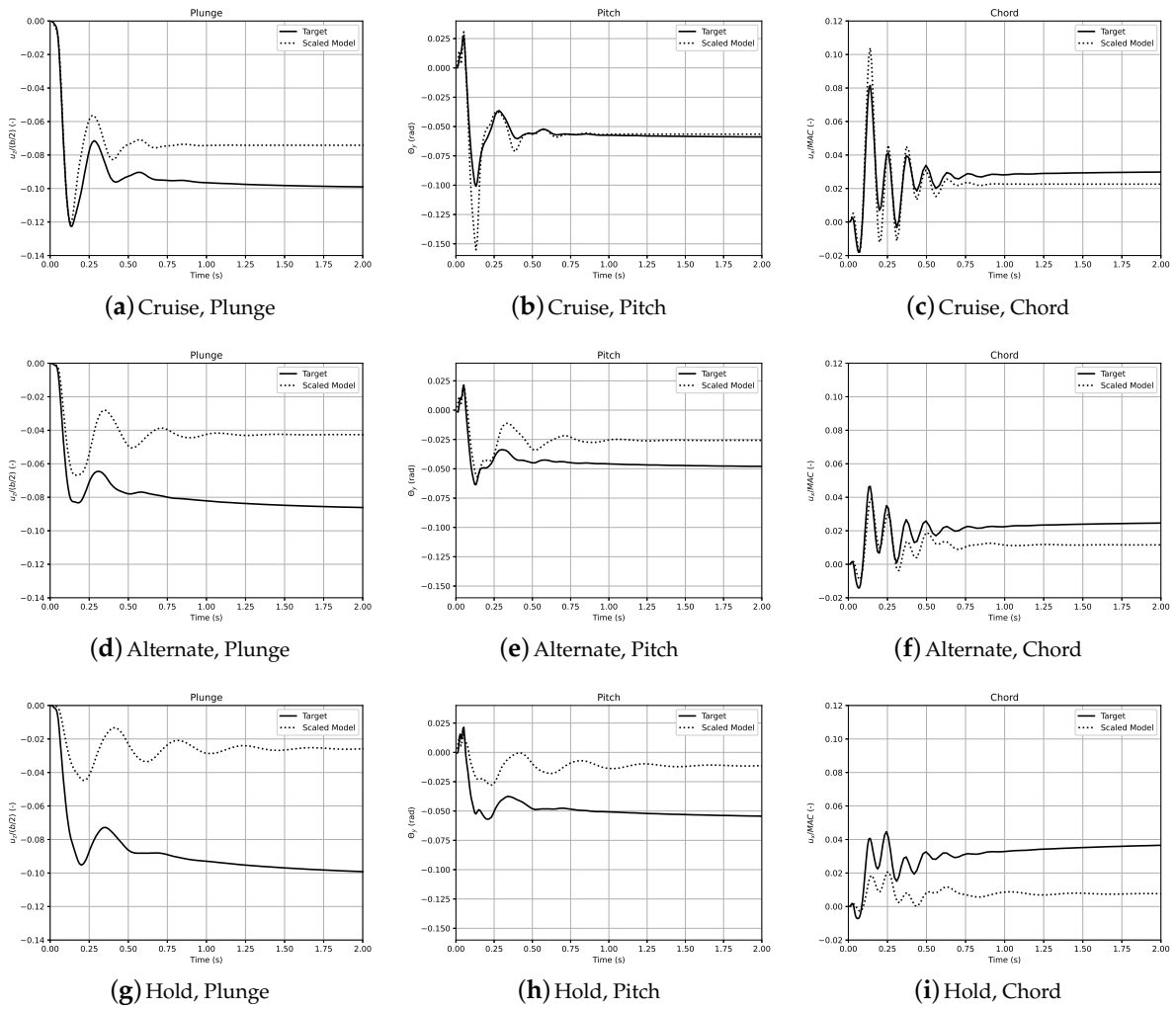


Figure 3. Aeroelastic response measure at the wing tip for plunge, pitch and chord degrees of freedom for the reduced and target models, considering SET 1.

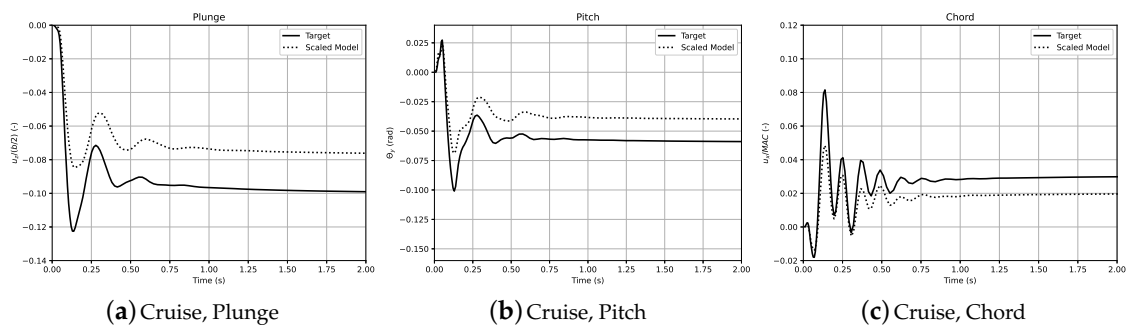


Figure 4. Cont.

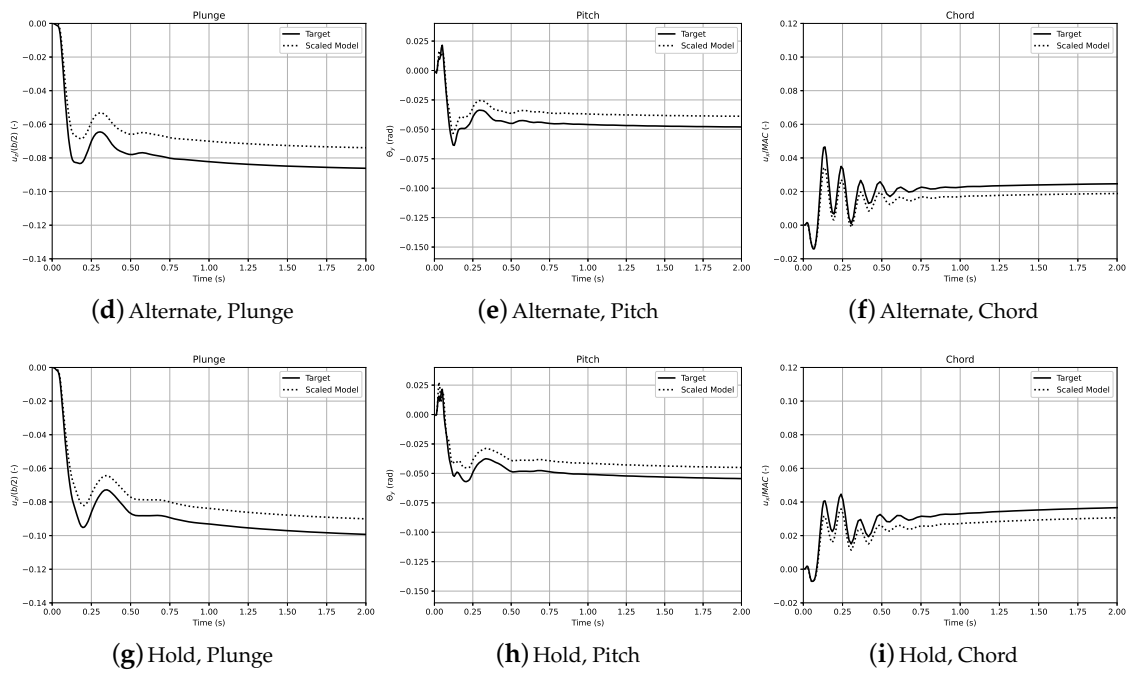


Figure 4. Aeroelastic response measure at the wing tip for plunge, pitch and chord degrees of freedom for the reduced and target models, considering SET 2.

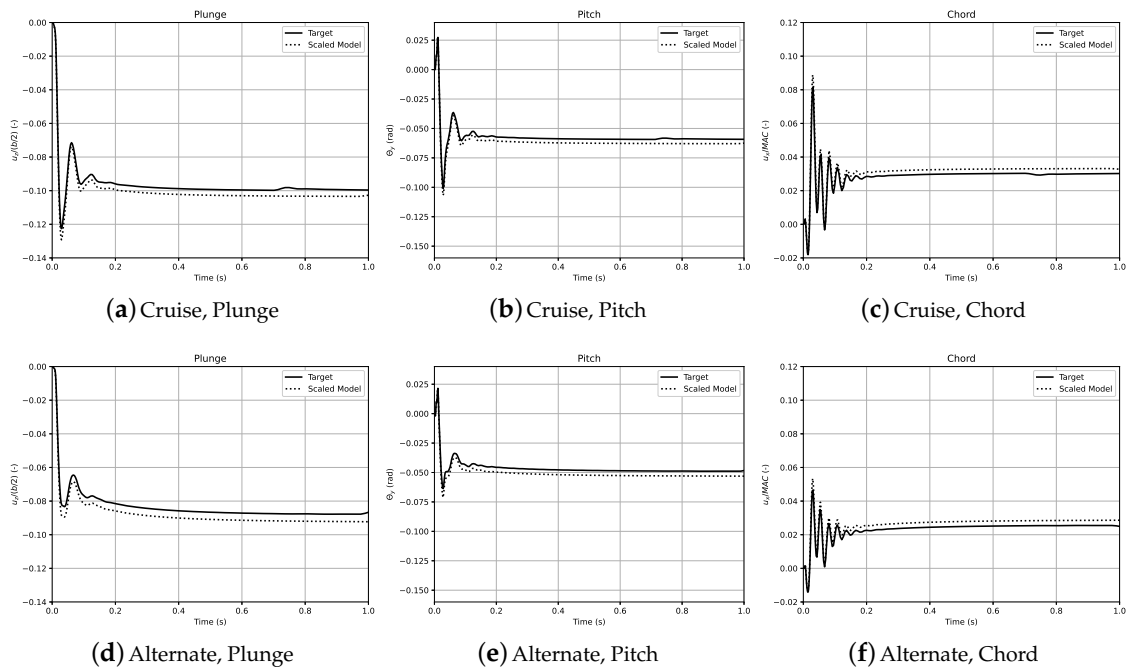


Figure 5. Cont.

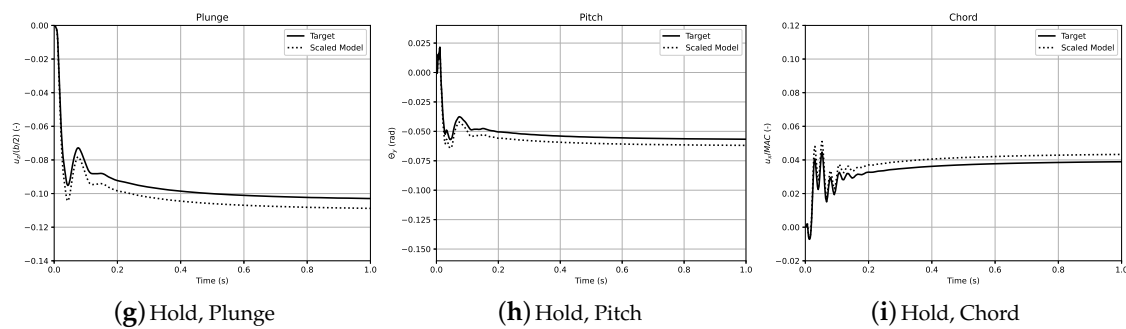


Figure 5. Aeroelastic response measure at the wing tip for plunge, pitch and chord degrees of freedom for the reduced and target models, considering SET 3.

5. Concluding Remarks

Three different strategies to formulate aeroelastically scaled models, based on several combinations of primary variables, were studied and compared for their aerodynamic, structural, inertial, and aeroelastic characteristics for different flight conditions. The first two sets (1 and 2) of primary quantities require solving an optimization problem to design the internal structure of the scaled model that matches the structural dynamic behavior (and inertial properties) of the full scale model. Set 3 represents an exact geometric scaling of the internal structure using the same material and it allows to promptly define the scaled structure without resorting to costly optimization methods.

In terms of aerodynamics, both Sets 1 and 2 perform poorly since neither Mach number nor Reynolds number are reproduceable in the scaled models due to the lower velocities and geometric sizes, when compared with the full size model. Mach number is matched in Set 3 thus improving the aerodynamic similarity between full and reduced models, while the Reynolds number is not maintained. Regarding structural dynamics and inertial properties, Set 3 outperforms the other sets since the direct scale down with the same material as the full size model is carried out. For the structural model and corresponding design variables defined in this work, Set 2 yields better agreement in natural frequencies when compared to Set 1. The better overall similarity (aerodynamic, structural and inertial) of Set 3 was also noticed in the nonlinear aeroelastic response (plunge, pitch and chord degrees of freedom measured at the wing tip), where good agreement between full and sub-scale models is observed independently of the flight condition, thus showing its potential for exploring the entire flight envelope.

Looking at the feasibility of devising the scaled models, Set 1 leads to designs that are easier to build and cheaper to test in both flight and wind tunnel, while it may only be suitable for a small variation of the flight condition and not the entire flight envelope. Models scaled using Set 2 should be easy to build as well, but they will probably be much more expensive to test since they require low air densities. Set 3 clearly exhibits better results and allows for an exploration of the entire flight envelope, although the exactly scaled down internal structure may be larger than most closed-loop wind tunnel test sections to ensure manufacturability.

Finally, the scaling strategies presented can be improved using higher fidelity aeroelastic tools that enable the study of other nonlinear aeroelastic phenomena such as shock waves along the wing span.

Author Contributions: Conceptualization, F.A., F.L. and A.S.; methodology, F.A. and M.C.; software, F.A. and J.V.; validation, F.A., J.V., F.L. and A.S.; formal analysis, F.A. and M.C.; investigation, F.A. and M.C.; data curation, F.A. and M.C.; writing—original draft preparation, F.A.; writing—review and editing, F.L. and A.S.; visualization, F.A.; supervision, F.L. and A.S.; project administration, F.L.; funding acquisition, A.S. All authors have read and agreed to the published version of the manuscript.

Funding: The authors acknowledge Fundação para a Ciência e a Tecnologia (FCT), through IDMEC, under LAETA, project UIDB/50022/2020.

Conflicts of Interest: The authors declare no conflict of interest.

Nomenclature

The following nomenclature is used in this manuscript:

$[A_C]$	aerodynamic damping matrix
$[A_K]$	aerodynamic stiffness matrix
$[A_M]$	aerodynamic mass matrix
b	wing span
$[C]$	damping matrix
k_M	moment scaling factors
f	frequency
F	force
Fr	Froude number
g	gravity acceleration
I	inertia
k	scaling factors
k_F	force scaling factors
k_I	inertia scaling factors
k_l	length scaling factors
k_m	mass scaling factors
k_M	moment scaling factors
k_p	pressure scaling factors
k_t	time scaling factors
k_v	velocity scaling factors
k_ρ	density scaling factors
k_ω	frequency scaling factors
$[K]$	stiffness matrix
m	mass
M	moment
$[M]$	mass matrix
Ma	Mach number
MAC	Modal Assurance Criteria
p	pressure
Re	Reynolds number
t	time
v	velocity
x	set of design variables
$\{x\}$	vector of displacements
$\{\dot{x}\}$	vector of velocities
$\{\ddot{x}\}$	vector of accelerations
κ	reduced frequency
ρ	density
ϕ	matrix with a set of mode shapes
ω	natural frequency

References

1. Patil, M.; Hodges, D. On the importance of aerodynamic and structural geometrical nonlinearities in aeroelastic behavior of high-aspect-ratio wings. *J. Fluids Struct.* **2004**, *19*, 905–915, doi:10.1016/j.jfluidstructs.2004.04.012.
2. Tang, D.; Dowell, E. Effects of geometric structural nonlinearity on flutter and limit cycle oscillations of high-aspect-ratio wings. *J. Fluids Struct.* **2004**, *19*, 291–306, doi:10.1016/j.jfluidstructs.2003.10.007.
3. Cesnik, C.E.; Palacios, R.; Reichenbach, E.Y. Reexamined Structural Design Procedures for Very Flexible Aircraft. *J. Aircr.* **2014**, *51*, 1580–1591, doi:10.2514/1.C032464.
4. Tsushima, N.; Su, W. Flutter suppression for highly flexible wings using passive and active piezoelectric effects. *Aerosp. Sci. Technol.* **2017**, *65*, 78–89, doi:10.1016/j.ast.2017.02.013.

5. de Souza Siqueira Versiani, T.; Silvestre, F.J.; Guimarães Neto, A.B.; Rade, D.A.; Annes da Silva, R.G.; Donadon, M.V.; Bertolin, R.M.; Silva, G.C. Gust load alleviation in a flexible smart idealized wing. *Aerosp. Sci. Technol.* **2019**, *86*, 762–774, doi:10.1016/j.ast.2019.01.058.
6. Modaress-Aval, A.H.; Bakhtiari-Nejad, F.; Dowell, E.H.; Peters, D.A.; Shahverdi, H. A comparative study of nonlinear aeroelastic models for high aspect ratio wings. *J. Fluids Struct.* **2019**, *85*, 249–274, doi:10.1016/j.jfluidstructs.2019.01.003.
7. Amato, E.; Polsinelli, C.; Cestino, E.; Frulla, G.; Joseph, N.; Carrese, R.; Marzocca, P. HALE wing experiments and computational models to predict nonlinear flutter and dynamic response. *Aeronaut. J.* **2019**, *123*, 912–946, doi:10.1017/aer.2019.38.
8. Cestino, E.; Frulla, G.; Spina, M.; Catelani, D.; Linari, M. Numerical simulation and experimental validation of slender wings flutter behaviour. *Proc. Inst. Mech. Eng. Part G J. Aerosp. Eng.* **2019**, *233*, 5913–5928, doi:10.1177/0954410019879820.
9. Riso, C.; Ghadami, A.; Cesnik, C.E.S.; Epureanu, B.I. Data-Driven Forecasting of Postflutter Responses of Geometrically Nonlinear Wings. *AIAA J.* **2020**, *58*, 2726–2736, doi:10.2514/1.J059024.
10. Afonso, F.; Vale, J.; Oliveira, É.; Lau, F.; Suleman, A. A review on non-linear aeroelasticity of high aspect-ratio wings. *Prog. Aerosp. Sci.* **2017**, *89*, 40–57, doi:10.1016/j.paerosci.2016.12.004.
11. Jonsson, E.; Riso, C.; Lupp, C.A.; Cesnik, C.E.; Martins, J.R.; Epureanu, B.I. Flutter and post-flutter constraints in aircraft design optimization. *Prog. Aerosp. Sci.* **2019**, *109*, 100537, doi:10.1016/j.paerosci.2019.04.001.
12. Gao, C.; Zhang, W. Transonic aeroelasticity: A new perspective from the fluid mode. *Prog. Aerosp. Sci.* **2020**, *113*, 100596, doi:10.1016/j.paerosci.2019.100596.
13. Coutinho, C.P.; Baptista, A.J.; Dias Rodrigues, J. Reduced scale models based on similitude theory: A review up to 2015. *Eng. Struct.* **2016**, *119*, 81–94, doi:10.1016/j.engstruct.2016.04.016.
14. Casaburo, A.; Petrone, G.; Franco, F.; De Rosa, S. A Review of Similitude Methods for Structural Engineering. *Appl. Mech. Rev.* **2019**, *71*, 030802, doi:10.1115/1.4043787.
15. Zhu, W. Models for wind tunnel tests based on additive manufacturing technology. *Prog. Aerosp. Sci.* **2019**, *110*, 100541, doi:10.1016/j.paerosci.2019.05.001.
16. Blair, M.; Garmann, D.; Canfield, R.; Bond, V.; Pereira, P.; Suleman, A. Non-Linear Aeroelastic Scaling of a Joined-Wing Concept. In Proceedings of the 48th AIAA/ASME/ASCE/AHS/ASC Structures, Structural Dynamics, and Materials Conference, Honolulu, HI, USA, 23–26 April 2007, doi:10.2514/6.2007-1887.
17. Richards, J.; Suleman, A. Aeroelastic scaling of unconventional joined wing concept for exploration of gust load response. In Proceedings of the International Forum on Aeroelasticity and Structural Dynamics IFASD, Seattle, WA, USA, 21–25 June, 2009.
18. Bond, V.L.; Canfield, R.A.; Suleman, A.; Blair, M. Aeroelastic Scaling of a Joined Wing for Nonlinear Geometric Stiffness. *AIAA J.* **2012**, *50*, 513–522, doi:10.2514/1.41139.
19. Wan, Z.; Cesnik, C.E.S. Geometrically Nonlinear Aeroelastic Scaling for Very Flexible Aircraft. *AIAA J.* **2014**, *52*, 2251–2260, doi:10.2514/1.J052855.
20. Pereira, P.; Almeida, L.; Suleman, A.; Bond, V.; Canfield, R.; Blair, M. Aeroelastic scaling and optimization of a joined wing aircraft concept. In Proceedings of the 48th AIAA/ASME/ASCE/AHS/ASC Structures, Structural Dynamics, and Materials Conference, Honolulu, HI, USA, 23–26 April 2007, doi:10.2514/6.2007-1889.
21. Coelho, M.; Afonso, F.; Lau, F.; Suleman, A. Nonlinear aeroelastic scaling studies on high aspect ratio wings. In Proceedings of the 6th EASN International Conference on Innovation in European Aeronautics Research, Porto, Portugal, 18–21 October, 2016.
22. Yusuf, S.Y.; Hayes, D.; Pontillo, A.; Carrizales, M.A.; Dussart, G.X.; Lone, M.M. Aeroelastic Scaling for Flexible High Aspect Ratio Wings. In Proceedings of the AIAA Scitech 2019 Forum, San Diego, CA, USA, 7–11 January 2019, doi:10.2514/6.2019-1594.
23. French, M. An application of structural optimization in wind tunnel model design. In Proceedings of the 31st Structures, Structural Dynamics and Materials Conference, Long Beach, CA, USA, 2–4 April 1990. doi:10.2514/6.1990-956.
24. French, M.; Eastep, F.E. Aeroelastic model design using parameter identification. *J. Aircr.* **1996**, *33*, 198–202, doi:10.2514/3.46922.
25. Ricciardi, A.P.; Eger, C.A.G.; Canfield, R.A.; Patil, M.J. Nonlinear Aeroelastic-Scaled-Model Optimization Using Equivalent Static Loads. *J. Aircr.* **2014**, *51*, 1842–1851, doi:10.2514/1.C032539.

26. Ricciardi, A.P.; Canfield, R.A.; Patil, M.J.; Lindsley, N. Nonlinear Aeroelastic Scaled-Model Design. *J. Aircr.* **2016**, *53*, 20–32, doi:10.2514/1.C033171.
27. Spada, C.; Afonso, F.; Lau, F.; Suleman, A. Nonlinear aeroelastic scaling of high aspect-ratio wings. *Aerosp. Sci. Technol.* **2017**, *63*, 363–371, doi:10.1016/j.ast.2017.01.010.
28. Banazadeh, A.; Hajipouzadeh, P. Using approximate similitude to design dynamic similar models. *Aerosp. Sci. Technol.* **2019**, *94*, 105375, doi:10.1016/j.ast.2019.105375.
29. Buckingham, E. On Physically Similar Systems; Illustrations of the Use of Dimensional Equations. *Phys. Rev.* **1914**, *4*, 345–376, doi:10.1103/PhysRev.4.345.
30. Ouellette, J.; Patil, M.; Kapania, R. Scaling Laws for Flight Control Development and Testing in the Presence of Aeroservoelastic Interactions. In Proceedings of the AIAA Atmospheric Flight Mechanics Conference, Minneapolis, MN, USA, 13–16 August 2012, doi:10.2514/6.2012-4640.
31. Pittit, C.L.; Canfield, R.A.; Ghanem, R.L. Stochastic analysis of a aeroelastic system. In Proceedings of the 15th ASCE Engineering Mechanics Conference, New York, NY, USA, 2–5 June 2002.
32. Bisplinghoff, R.L.; Ashley, H.; Halfman, R.L. *Aeroelasticity*; Dover Publications: Mineola, NY, USA, 1996.
33. Suleman, A.; Afonso, F.; Vale, J.; Oliveira, E.; Lau, F. Non-linear aeroelastic analysis in the time domain of high-aspect-ratio wings: Effect of chord and taper-ratio variation. *Aeronaut. J.* **2017**, *121*, 21–53, doi:10.1017/aer.2016.94.
34. Afonso, F.; Leal, G.; Vale, J.; Oliveira, E.; Lau, F.; Suleman, A. The effect of stiffness and geometric parameters on the nonlinear aeroelastic performance of high aspect ratio wings. *Proc. Inst. Mech. Eng. Part G J. Aerosp. Eng.* **2017**, *231*, 1824–1850, doi:10.1177/0954410016675893.
35. Howcroft, C.; Neild, S.; Lowenberg, M.; Cooper, J. Efficient aeroelastic beam modelling and the selection of a structural shape basis. *Int. J. Non-Linear Mech.* **2019**, *112*, 73–84, doi:10.1016/j.ijnonlinmec.2018.11.007.
36. Rajpal, D.; Gillebaart, E.; De Breuker, R. Preliminary aeroelastic design of composite wings subjected to critical gust loads. *Aerosp. Sci. Technol.* **2019**, *85*, 96–112, doi:10.1016/j.ast.2018.11.051.
37. Afonso, F.; Vale, J.; Lau, F.; Suleman, A. Performance based multidisciplinary design optimization of morphing aircraft. *Aerosp. Sci. Technol.* **2017**, *67*, 1–12, doi:10.1016/j.ast.2017.03.029.
38. De Gaspari, A.; Ricci, S.; Antunes, A.; Odaguil, F.; Lima, G. Chapter 6-Expected Performances. In *Morphing Wing Technologies*; Concilio, A., Dimino, I., Lecce, L., Pecora, R., Eds.; Butterworth-Heinemann: Oxford, UK, 2018; pp. 175–203, doi:10.1016/B978-0-08-100964-2.00006-X.
39. Ngo, T.D.; Kashani, A.; Imbalzano, G.; Nguyen, K.T.; Hui, D. Additive manufacturing (3D printing): A review of materials, methods, applications and challenges. *Compos. Part B Eng.* **2018**, *143*, 172–196, doi:10.1016/j.compositesb.2018.02.012.
40. Zhu, W.; Zhang, X.; Li, D. Flexible all-plastic aircraft models built by additive manufacturing for transonic wind tunnel tests. *Aerosp. Sci. Technol.* **2019**, *84*, 237–244, doi:10.1016/j.ast.2018.10.024.

Publisher’s Note: MDPI stays neutral with regard to jurisdictional claims in published maps and institutional affiliations.



© 2020 by the authors. Licensee MDPI, Basel, Switzerland. This article is an open access article distributed under the terms and conditions of the Creative Commons Attribution (CC BY) license (<http://creativecommons.org/licenses/by/4.0/>).